Optical-plug-assisted spin vortex in a ^{87}Rb dipolar spinor Bose-Einstein condensate

Hui Tang [1], Peng Du [1], Lei Jing [1], Su Yi [2,3] and Wenxian Zhang [1,4,*]

[1] *Key Laboratory of Artificial Micro- and Nano-structures of Ministry of Education, School of Physics and Technology, Wuhan University, Wuhan, Hubei 430072, China*

[2] *CAS Key Laboratory of Theoretical Physics, Institute of Theoretical Physics, Chinese Academy of Sciences, P.O. Box 2735, Beijing 100190, China*

[3] *School of Physical Sciences and CAS Center for Excellence in Topological Quantum Computation, University of Chinese Academy of Sciences, Beijing 100049, China*

[4] *Wuhan Institute of Quantum Technology, Wuhan, Hubei 430206, China*

(Received 7 April 2022; accepted 15 June 2022; published 23 June 2022; corrected 1 July 2022)

Generating a spin vortex in a ^{87}Rb dipolar spinor Bose-Einstein condensate in a controllable way is still experimentally challenging. We propose an experimentally easy and tunable way to produce a spin vortex by varying the potential barrier height and the width of an additionally applied optical plug. A topological phase transition occurs from the trivial single-mode approximation phase to the optical-plug-assisted-vortex one, as the barrier height increases and the width lies in an appropriate range. The optical plug causes radial density variation and thus the spin vortex is favored by significantly lowering the intrinsic magnetic dipolar energy. A type of coreless spin vortex, different from the conventional polar core vortex, is predicted by our numerical results. Our proposal removes a major obstacle to investigating the topological phase transition in a ^{87}Rb dipolar spinor Bose-Einstein condensate.

DOI: 10.1103/PhysRevA.105.063324

I. INTRODUCTION

Phase transitions are ubiquitous in the classical world [1], while in the quantum world, phase transitions are an important and developing branch of quantum theory, especially for unconventional topological phase transitions and dynamical quantum phase transitions. Although various types of quantum phase transitions have been observed for decades in many quantum systems, such as superconducting phase transitions, magnetic phase transitions, and quantum Hall phase transitions [2–6], quantum phase transitions in a controllable way have become possible only recently, with the aid of fine-tuning quantum control techniques developed in the past 20 years [7–9].

The Bose-Einstein condensate (BEC) in alkali-metal atomic gases offers an excellent platform for the experimental investigation of quantum phase transitions, due to its extremely clean environment, macroscopical quantum behaviors, and great controllability. In particular, when the optical potential was first utilized to trap the atomic gases, a vast unexplored area in the ultracold atomic physics was opened up by revealing the spin degree of freedom [10]. Beautiful theories and extensive experimental investigations of spinor BECs have been developed and subsequently carried out [11–18].

It has been well known that there exist two kinds of spin interaction in a dipolar spinor condensate: the short-range and isotropic spin-exchange interaction and the long-range and anisotropic magnetic dipole-dipole interaction (MDDI) [19–26]. The competition between these two spin interactions drives the system into a rich spin phase diagram, e.g., from the ferromagnetic phase to the antiferromagnetic one by changing the spin-exchange interaction and from the spin-uniform single-mode approximation (SMA) phase to the polar core vortex (PCV) one by increasing the MDDI strength [27–29].

Among these phase transitions, the topological phase transition is of particular interest due to its sudden change of the global property at the critical point. It also offers a new paradigm of quantum phase transition. For a metastable state, topological vortices and spin domains were pursued experimentally and numerically with large-scale supercomputers through quench dynamics in a ^{87}Rb dipolar spinor condensate [25,30,31]. For the ground state, however, the topological phase transition from the SMA to the PCV was only predicted theoretically and confirmed numerically in a dipolar spinor BEC. It has yet been realized in experiments [27,28]. The conditions to generate such a ground-state spin vortex are rather challenging, both with a highly anisotropic trap potential and with an extremely large number of atoms. A more controllable manner and less stringent experimental conditions to realize the topological phase transitions are still seriously needed.

In this paper we apply an additional optical plug to a ^{87}Rb dipolar spinor BEC in a highly anisotropic pancake optical trap [32–34]. By varying the potential barrier height and the width of the optical plug, we expect to realize the topological phase transition in the ^{87}Rb condensate with fewer atoms and a lower experimentally available trap aspect ratio. With analytical arguments and numerical calculations, we illustrate the phase transition from the SMA to the optical-plug-assisted spin vortex, due to the competition between the MDDI and the

*Corresponding author: wxzhang@whu.edu.cn

kinetic energy with the optical plug. The generated spin vortex is further divided into two cases: a PCV and a flux-closure coreless spin vortex (FCLSV). Actually, the FCLSV has a similar spin structure to the PCV but the polar core is strongly suppressed by the optical plug. Our results reveal a viable and tunable way to experimentally investigate the topological quantum phase transition in a ^{87}Rb dipolar spinor condensate.

The paper is organized as follows. We describe the nonlocal model with the coupled Gross-Pitaevskii equations (GPEs) for the ^{87}Rb dipolar spinor BEC in Sec. II. We sketch the idea and the analytical arguments of generating a spin vortex with the application of an additional optical plug in Sec. III. In Secs. IV and V we describe the numerical truncation technique for the accurate calculation of the MDDI in the condensate and present the numerical results which confirm the topological phase transition from the SMA to the spin vortex, respectively. A summary is given in Sec. VI.

II. NONLOCAL DIPOLAR MODEL

Due to the long-range nature of its MDDI, a ^{87}Rb dipolar spin-1 BEC in an optical trap is described by a nonlocal model. The Hamiltonian in the second quantized form is [23,28,35,36]

$$\begin{aligned}\hat{H} = \int d\mathbf{r}\Big[&\hat{\psi}_\alpha^\dagger(\mathbf{r})\Big(-\frac{\hbar^2\nabla^2}{2M}+V(\mathbf{r})\Big)\hat{\psi}_\alpha(\mathbf{r})\\&+\frac{c_0}{2}\hat{\psi}_\alpha^\dagger(\mathbf{r})\hat{\psi}_\beta^\dagger(\mathbf{r})\hat{\psi}_\beta(\mathbf{r})\hat{\psi}_\alpha(\mathbf{r})\\&+\frac{c_2}{2}\hat{\psi}_\alpha^\dagger(\mathbf{r})\hat{\psi}_{\alpha'}^\dagger(\mathbf{r})\mathbf{F}_{\alpha\beta}\cdot\mathbf{F}_{\alpha'\beta'}\hat{\psi}_\beta(\mathbf{r})\hat{\psi}_{\beta'}(\mathbf{r})\Big]\\&+\hat{H}_{dd},\end{aligned} \tag{1}$$

where $\hat{\psi}_\alpha$ ($\alpha = 0, \pm 1$) represents the annihilation operator in the magnetic level α, M the mass of a ^{87}Rb atom, and $\mathbf{F}_{\alpha\beta}$ the spin-1 matrix. The spin-independent interaction strength is $c_0 = 4\pi\hbar^2(a_0 + 2a_2)/3M$ and the spin-dependent exchange interaction is $c_2 = 4\pi\hbar^2(a_2 - a_0)/3M$, which originate from the two-body s-wave scattering with a_s ($s = 0, 2$) the characteristic scattering length of the total spin s.

The $V(\mathbf{r})$ is an external harmonic trap with an additional optical plug,

$$V(\mathbf{r}) = \tfrac{1}{2}M\omega_0^2(x^2+y^2+\lambda^2z^2) + U_0e^{-(x^2+y^2)/\sigma^2}, \tag{2}$$

where ω_0 is the harmonic trap angular frequency in the x-y plane, λ is the trap aspect ratio, and U_0 and σ are two adjustable parameters characterizing the barrier height and the width of the Gaussian optical plug, respectively [32–34]. The Hamiltonian of the MDDI $\hat{H}_{dd}$ is

$$\begin{aligned}\hat{H}_{dd} = \frac{c_{dd}}{2}\int d\mathbf{r}\int d\mathbf{r}'\frac{1}{|\mathbf{r}-\mathbf{r}'|^3}\\\times[\hat{\psi}_\alpha^\dagger(\mathbf{r})\hat{\psi}_{\alpha'}^\dagger(\mathbf{r})\mathbf{F}_{\alpha\beta}\cdot\mathbf{F}_{\alpha'\beta'}\hat{\psi}_\beta(\mathbf{r})\hat{\psi}_{\beta'}(\mathbf{r})\\-3\hat{\psi}_\alpha^\dagger(\mathbf{r})\hat{\psi}_{\alpha'}^\dagger(\mathbf{r})(\mathbf{F}_{\alpha\beta}\cdot\mathbf{e})(\mathbf{F}_{\alpha'\beta'}\cdot\mathbf{e})\hat{\psi}_\beta(\mathbf{r})\hat{\psi}_{\beta'}(\mathbf{r})],\end{aligned} \tag{3}$$

where $c_{dd} = \mu_0 g_F^2\mu_B^2/4\pi$, with μ_0 the magnetic permeability of the vacuum, g_F the Landé g factor for the ^{87}Rb atom, and μ_B the Bohr magneton, and $\mathbf{e} = (\mathbf{r}-\mathbf{r}')/|\mathbf{r}-\mathbf{r}'|$ is the unit vector along $\mathbf{r}-\mathbf{r}'$.

By adopting the standard mean-field approximation [16], the order parameter (wave function) of the dipolar spin-1 BEC becomes $\Psi(\mathbf{r}) = (\psi_1(\mathbf{r}), \psi_0(\mathbf{r}), \psi_{-1}(\mathbf{r}))^T$. The dynamics of the system is described by the nonlocal GPEs [37,38]

$$i\hbar\frac{\partial\psi_\alpha(\mathbf{r})}{\partial t} = (T+V+c_0n)\psi_\alpha + \mathbf{B}_e\cdot\mathbf{F}_{\alpha\beta}\psi_\beta, \tag{4}$$

where $T = -\hbar^2\nabla^2/2M$ and $n = \sum_\alpha|\psi_\alpha|^2$ the total density. All spin-dependent interactions are considered as an effective magnetic field

$$\mathbf{B}_e(\mathbf{r}) = c_2\mathbf{f}(\mathbf{r}) + c_{dd}\mathbf{D}(\mathbf{r}), \tag{5}$$

where $\mathbf{f}(\mathbf{r}) = \sum_{\alpha\beta}\psi_\alpha^*(\mathbf{F}_{\alpha\beta})\psi_\beta$ is the spin density and $\mathbf{D}(\mathbf{r})$ denotes dipolar contribution with its $\mu(\mu = x, y, z)$ component defined as

$$D_\mu(\mathbf{r}) = -\sum_{\nu=x,y,z}\int d\mathbf{r}'\frac{(\delta_{\mu\nu}-3e_\mu e_\nu)\mathbf{f}_\nu(\mathbf{r}')}{|\mathbf{r}-\mathbf{r}'|^3}. \tag{6}$$

In the numerical calculation, we also employ

$$\begin{aligned}D_+(\mathbf{r}) = D_-^*(\mathbf{r}) &= D_x(\mathbf{r}) + iD_y(\mathbf{r})\\&= \frac{3}{2}\int d\mathbf{r}'\frac{\sin^2\theta e^{i2\varphi}\mathbf{f}_-(\mathbf{r}')}{|\mathbf{r}-\mathbf{r}'|^3}\\&\quad+\frac{1}{2}\int d\mathbf{r}'\frac{(1-3\cos^2\theta)\mathbf{f}_+(\mathbf{r}')}{|\mathbf{r}-\mathbf{r}'|^3}+\frac{3}{2}\int d\mathbf{r}'\\&\quad+\frac{\sin 2\theta e^{i\varphi}\mathbf{f}_z(\mathbf{r}')}{|\mathbf{r}-\mathbf{r}'|^3},\end{aligned} \tag{7}$$

where $\mathbf{f}_+ = \mathbf{f}_-{}^* = \mathbf{f}_x + i\mathbf{f}_y$. The polar and azimuthal angles of the unit vector $\mathbf{e}$ are θ and φ, respectively. For numerical convenience, we set the length unit as $a_r = \sqrt{\hbar/M\omega_0}$, the energy unit as $E_0 = \hbar\omega_0$, and the density unit as $n_r = N/a_r^3$.

For a set of parameters $\{U_0, \sigma\}$ of the optical plug, we can find the ground state of the dipolar spin-1 BEC by solving Eq. (4) with the imaginary-time propagation method [39,40]. The phase diagram is obtained by scanning U_0 and σ and the phase transition and optical-plug-induced vortex are then investigated. We do not expect that a tiny external magnetic field much smaller than $|\mathbf{B}_e|$ would change qualitatively the results.

III. OPTICAL-PLUG-ASSISTED SPIN VORTEX

The spin vortex in a dipolar spinor BEC has been investigated extensively in theory and experiment [25,28–30,35]. We first briefly review a special spin vortex, the PCV [16,41–44].

In general, the ground state of a ^{87}Rb dipolar spinor BEC is a ferromagnetic SMA phase, due to $|c_2| \gg c_{dd}$ and $c_2 < 0$, where all three components share the same spatial mode. The energy of such a SMA state is

$$E^S = T + V + E_0 + E_2 + E_{dd}, \tag{8}$$

where T, V, and E_0 are the kinetic energy, the trap potential energy, and the spin-independent energy, respectively. The spin energy includes the spin-exchange energy E_2 and the weak but long-range MDDI energy E_{dd}. It is easy to obtain that [16,45]

$$E_{dd} = E'_{dd} + E''_{dd}, \tag{9}$$

with

$$E'_{dd} = \frac{1}{4\pi^2} c_{dd} \int d\boldsymbol{k} |\hat{\boldsymbol{k}} \cdot \tilde{\boldsymbol{f}}(\boldsymbol{k})|^2,$$
$$E''_{dd} = -\frac{2\pi}{3} c_{dd} \int d\boldsymbol{r} |\boldsymbol{f}(\boldsymbol{r})|^2,$$

where $\tilde{\boldsymbol{f}}(\mathbf{k})$ is the Fourier transform of the spin density $f(\mathbf{r})$ and $\int d\boldsymbol{k} |\tilde{\boldsymbol{f}}(\boldsymbol{k})|^2 = (2\pi)^3 \int d\boldsymbol{r} |\boldsymbol{f}(\mathbf{r})|^2$. We find immediately that E''_{dd} shares the same form as $E_2 \equiv (c_2/2) \int d\mathbf{r} |\boldsymbol{f}(\mathbf{r})|^2$, so we define an equivalent spin-exchange energy

$$E'_2 = E_2 + E''_{dd} = (1 + p) E_2,$$

where $p \equiv E''_{dd}/E_2 = 4\pi c_{dd}/3|c_2| \approx 0.3797$ for a ^{87}Rb BEC.

Similarly, for a PCV state, its energy E^V is almost the same except for the energy difference from the local area around the vortex core and the dipolar energy difference from the spin structure. Clearly, for a uniform and large BEC (compared to the core size of a spin vortex), the long-range dipolar energy would dominate the spin (vortex) structure because other terms are local and negligible. We thus analyze the MDDI energy difference between the SMA and the PCV state, $\Delta E = E^V - E^S \approx E'^V_{dd} - E'^S_{dd}$, where E'^S_{dd} and E'^V_{dd} are the intrinsic MDDI energies for the SMA and the PCV state, respectively. It is easy to find that $\Delta E < 0$ because $E'^V_{dd} = 0$, due to the circular spin density structure $\hat{\boldsymbol{k}} \cdot \tilde{\boldsymbol{f}}(\boldsymbol{k}) = 0$ [16,28], and $E'^S_{dd} > 0$. Consequently, the PCV state may become the ground state. In fact, Kawaguchi and Ueda found that the PCV state is indeed the ground state if the MDDI is strong enough for a dipolar spinor condensate with the atom number larger than a threshold N_c [16].

Although the PCV state may be the ground state for a large enough dipolar condensate, the condition to observe such a spin texture in a finite-size BEC is still quite challenging, e.g., the atom number threshold $N_c \sim 2.6 \times 10^6$ for a spherical trap with $\omega_0 = 2\pi \times 100$ Hz. Even for a disk trap with $\lambda = 20$, the threshold is still $N_c \sim 1.4 \times 10^6$. To mitigate these stringent requirements, we propose placing an optical plug at the center of the BEC. This idea is inspired by the observation that a nonzero density gradient helps the formation of the PCV structure by lowering the term E'_{dd} [46].

Let us consider a limiting case, a quasi-one-dimensional ring trap formed by a harmonic trap and an optical plug with a width σ and an infinite barrier height [47]. Obviously, such a spin vortex is coreless since the total density is zero due to the infinite barrier height. For the FCLSV, we compare the energy difference(per atom) ΔE between the spin vortex and the SMA state. Obviously, we find

$$\Delta E = \Delta T + \Delta E'_{dd}$$

since other terms are the same for both states. We have defined $\Delta T = T^V - T^S$ with $T^{V,S}$ the kinetic energy for the spin vortex and the SMA state, respectively. After a straightforward calculation we find

$$\Delta E = \frac{\zeta_1 + \zeta_{-1}}{2\sigma^2} - \frac{c_{dd} N}{8\pi\sigma^3} I_{dd}, \tag{10}$$

where $\zeta_m = N_m/N$, with N_m the atom number of m component, and I_{dd} is a constant independent of σ defined by

$$I_{dd} = \int_{\varphi_c}^{2\pi - \varphi_c} d\varphi \frac{3 - 2\sin^2(\varphi)}{|\sin(\varphi)|^3},$$

with φ_c the cutoff (smallest) angle. The cutoff angle is on the order of $\varphi_c \sim r_0/\sigma$, with r_0 the average distance between two closest atoms on the ring [40,48–52]. We have used $T^S = 0$ (see the Appendix for the derivation).

As shown by Eq. (10), the energy difference ΔE is lowered as σ decreases and may be negative if σ is smaller than a characteristic width $\sigma_c = c_{dd} N I_{dd}/4(\zeta_1 + \zeta_{-1})$. The ground state becomes a spin vortex. Of course, the optical-plug width should be larger than the dipolar healing length ξ_{dd} in order to form a vortex $\sigma > \xi_{dd}$, with $\xi_{dd} = \hbar/\sqrt{2M c_{dd} n}$ and n the characteristic density [28,35]. Based on the above analysis, we may draw the conclusion that the application of an optical plug may help form a spin vortex in a dipolar spinor BEC.

IV. TRUNCATION EFFECT OF MDDI

Accurately calculating the dipolar potential $D_{x,y,z}$ is numerically time consuming, due to the nonlocal nature of the MDDI and the multidimensional integral in the real space. A conventional method to overcome this difficulty is employing the fast Fourier transform (FFT) convolution theorem [40,53]. However, the introduction of the FFT causes quite a large error because the FFT approach assumes a periodic lattice which is not a good approximation in a trapped dipolar BEC. Thus, the MDDI must be truncated to increase the numerical accuracy, particularly in the tightest trapped direction, as in a polarized dipolar BEC [54].

We restrict the dipole potential to the z direction with $|z - z'| < |R_z|$ by applying a window function to the integral kernel terms with $(\delta_{\mu\nu} - 3e_\mu e_\nu)/|\mathbf{r} - \mathbf{r}'|^3$ [35,48]. The window function and its Fourier transform are

$$W(z) = \begin{cases} 1, & |z| < R_z \\ 0, & |z| > R_z \end{cases} \tag{11}$$

and

$$\tilde{W}(k_z) = \frac{\sin(R_z k_z)}{\pi k_z}. \tag{12}$$

respectively. The kernel terms now become

$$y_{22}(\mathbf{r} - \mathbf{r}') = \frac{\sin^2\theta e^{i2\varphi}}{|\mathbf{r} - \mathbf{r}'|^3} W(|z - z'|),$$
$$y_{21}(\mathbf{r} - \mathbf{r}') = \frac{\sin 2\theta e^{-i\varphi}}{|\mathbf{r} - \mathbf{r}'|^3} W(|z - z'|),$$
$$y_{20}(\mathbf{r} - \mathbf{r}') = \frac{1 - 3\cos^2\theta}{|\mathbf{r} - \mathbf{r}'|^3} W(|z - z'|). \tag{13}$$

TABLE I. Relative error of the MDDI energy before and after truncation. The relative error is an order of magnitude smaller with the truncation method. The grid points are $128 \times 128 \times 64$ along the x, y, and z axes, respectively.

λ	10	20	40	60	80
$R_{x,y}$	8	8	11	15	22.5
R_z	4.5	3.25	3	2.5	1.5
ε_o	1.4×10^{-2}	2.3×10^{-2}	1.9×10^{-2}	2.4×10^{-2}	6.9×10^{-2}
ε_t	4.7×10^{-3}	5.4×10^{-3}	2.4×10^{-3}	2.5×10^{-3}	9.6×10^{-3}

After the FFT, these terms are

$$\begin{aligned}\tilde{y}_{22}(k) =& -\frac{4\pi}{3}\sin\alpha e^{i2\beta}[\sin\alpha - \sin\alpha\cos(R_z k_z)e^{-R_z k_\perp} \\ &+ \cos\alpha\sin(R_z k_z)e^{-R_z k_\perp}], \\ \tilde{y}_{21}(k) =& -\frac{8\pi}{3}\sin\alpha e^{i\beta}[\cos\alpha - \cos\alpha\cos(R_z k_z)e^{-R_z k_\perp} \\ &- \sin\alpha\sin(R_z k_z)e^{-R_z k_\perp}], \\ \tilde{y}_{20}(k) =& -\frac{4\pi}{3}(1-3\cos^2\alpha) + 4\pi e^{-R_z k_\perp}[\sin^2\alpha\cos(R_z k_z) \\ &- \sin\alpha\cos\alpha\sin(R_z k_z)],\end{aligned} \tag{14}$$

where $k_\perp = \sqrt{k_x^2 + k_y^2}$, α is the polar angle, and β is the azimuthal angle of the unit vector $\hat{k}$.

We evaluate the dipolar energy on the cubic grids of extent $[-R_x, R_x] \times [-R_y, R_y] \times [-R_z, R_z]$. The calculation box is lager than the condensate size, i.e., $R_{x,y,z} \sim 1.5 \times R^c_{x,y,z}$. The condensate size is defined as $n(R^c_x, R^c_y, R^c_z) = 10^{-9} \times n_p$, with n_p the highest density. Note that the truncation size coincides with the calculation box along z axis. In order to obtain valid results, the truncation window $[-R_z, R_z]$ must be larger than the condensate size. Combining Eqs. (14) and (9), we calculate the dipolar energy in three ways: the original method, the truncated numerical method, and the analytical method for a given quantum state of the spin-1 condensate. The wave function has the form $\psi_m(\mathbf{r}) = \sqrt{n(\mathbf{r})/3}$ with the density

$$n(\mathbf{r}) = \sqrt{\frac{\lambda}{(2\pi)^3}}\exp[-(x^2 + y^2 + \lambda z^2)/2]. \tag{15}$$

We denote by E_a the analytical MDDI energy, by E_o the original, and by E_t the truncated. The relative errors are defined as $\varepsilon_v = |(E_v - E_a)/E_a|$ $(v = o, t)$. The results are displayed in Table I. Clearly, although we may in principle reduce the relative error by simply extending the computation range with more grid points, the truncation operation is a more efficient and practical way.

V. NUMERICAL RESULTS ON TOPOLOGICAL PHASE TRANSITION

We determine numerically the ground state of the ^{87}Rb dipolar spin-1 condensate by employing the conventional operator-splitting approach to evolve the three coupled GPEs (4) in the imaginary-time domain. The kinetic and the truncated MDDI terms are calculated with the FFT algorithm [55]. We set the atom number in the condensate as $N = 5 \times 10^5$, the trap frequency $\omega_0 = 2\pi \times 100$ Hz, the trap aspect ratio $\lambda = 20$, and the calculation box $R_x = R_y = 27a_r$ and $R_z = 2.8a_r$, unless stated otherwise. The two optical-plug parameters, the barrier height U_0 and the width σ, are scanned. The initial wave function is set as a parabolic shape with random coefficients.

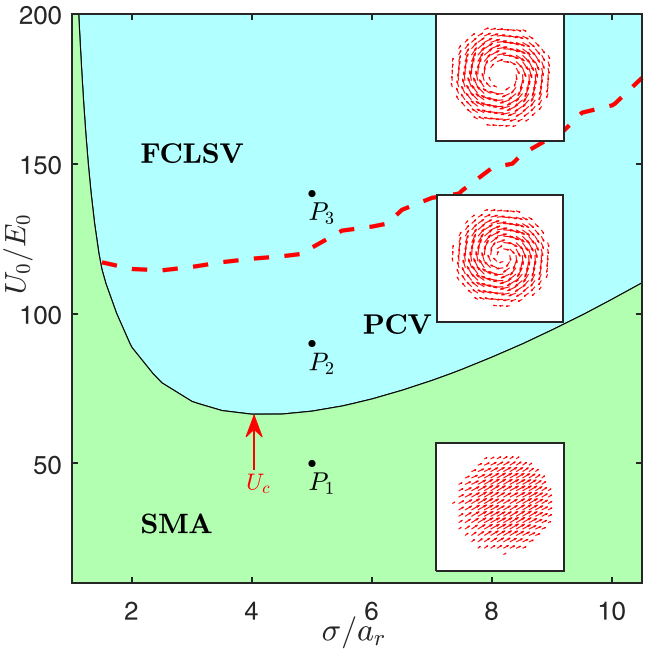

FIG. 1. Phase diagram of a ^{87}Rb dipolar BEC with an optical plug. The spin vortex phase emerges when the optical-plug barrier height U_0 and the width σ lie in the cyan region. Within the spin vortex phase, the FCLSV appears if the parameter (U_0, σ) is above the dashed red line and the PCV appears below. The top inset sketches the spin density distribution in the x-y plane for the FCLSV ground state at the parameter P_3. The middle inset shows that for the PCV ground state at P_2. The bottom inset portrays that for the SMA ground state at P_1. The other parameters are $\lambda = 20$ and $N = 5 \times 10^5$.

The phase diagram in the parameter space (U_0, σ), as shown in Fig. 1, summarizes the key results for the dipolar spinor ^{87}Rb BEC. We observe that two phases are present, the SMA and the spin vortex phases, whose spin density distributions are sketched in the insets in Fig. 1. From the figure we find that the appearance of the spin vortex phase requires the optical-plug barrier height to be larger than a critical value $U_0 > U_c$. Once the U_0 is large enough, the optical-plug width σ also has to be in an appropriate range, neither too big nor too small, for the spin vortex phase. This numerical result agrees qualitatively with the previous analysis in Sec. III, where the width should lie in an intermediate range. Interestingly, we find a spin structural change within the spin vortex phase, from the PCV to the FCLSV, which is coreless (the nearly zero total density or numerically the total density at the center is less than 1% of the peak density). The spin structural change is marked by the red dashed line in Fig. 1. We note that this is not a phase transition because the symmetries are the same in the PCV and the FCLSV region [38].

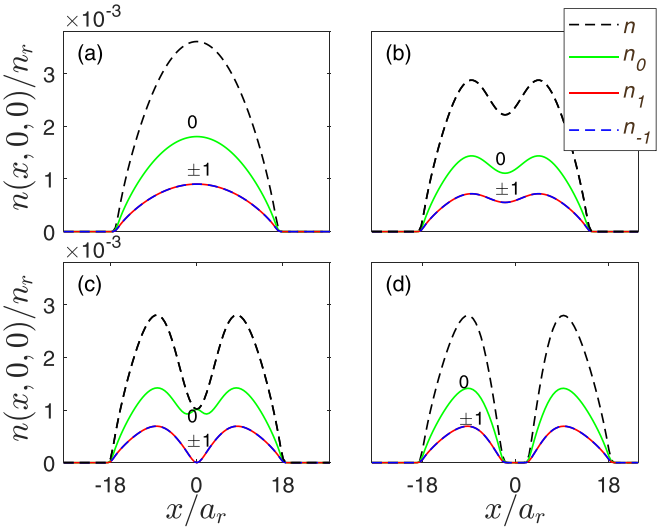

FIG. 2. Density distribution of the ground state on the x axis ($y = 0$ and $z = 0$) for the total density n (black dashed line) and three components n_1 (red solid line), n_0 (green solid line), and n_{-1} (blue dashed line). The optical-plug potential height is (a) $U_0 = 0$, (b) $U_0 = 50$, (c) $U_0 = 90$, and (d) $U_0 = 140$. The other parameters are $\sigma = 5$, $\lambda = 20$, and $N = 5 \times 10^5$. (b)–(d) correspond to the parameters P_1, P_2, and P_3 in Fig. 1, respectively. (a) and (b) belong to the SMA phase where the wave function of three components share the same spatial mode. (c) and (d) belong to the PCV and the FCLSV, respectively.

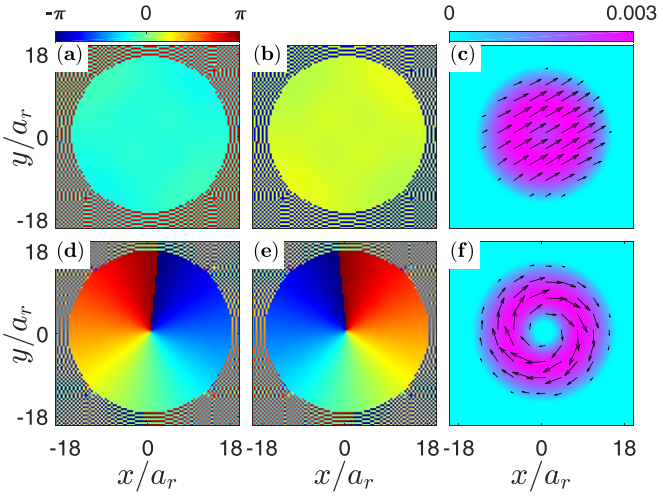

FIG. 3. Spatial phase distribution of the ground state in the x-y plane ($z = 0$) for (a) the $|+1\rangle$ component and (b) the $|-1\rangle$ component, with $U_0 = 50$ (P_1, the SMA state in Fig. 1). (d) and (e) Same as (a) and (b) except with $U_0 = 140$ (P_3, the FCLSV state). (c) and (f) Corresponding spin density (arrows) at P_1 and P_3, respectively. The color denotes the total density n. The other parameters are the same as in Fig. 2.

The ground-state density is significantly suppressed by the optical plug, as shown in Fig. 2. The figure shows only the density distribution along the x axis because the density distribution is cylindrically symmetric. As the optical-plug barrier height U_0 increases, the total density within and around the optical plug becomes lower until it reaches nearly zero. Correspondingly, the densities of each spin component show a similar trend. An interesting feature is also exhibited, i.e., the density distributions of the $|m_F = +1\rangle$ and $|m_F = -1\rangle$ components are exactly the same $n_1(\mathbf{r}) = n_{-1}(\mathbf{r})$. The phenomenon of $f_z(\mathbf{r}) = n_1 - n_{-1} = 0$ manifests the anisotropic property of the MDDI, i.e., spins are aligned in the easy plane, which is the x-y plane for a disk-shaped condensate with $\lambda \gg 1$ [27,35,36]. In addition, we find that the density of the $|m_F = 0\rangle$ component $n_0(\mathbf{r})$ is always larger than $n_1(\mathbf{r})$ and $n_{-1}(\mathbf{r})$ and $n_0(\mathbf{r}) \approx 2n_1(\mathbf{r})$ in the SMA and the FCLSV phases (not in the PCV). These features stem from the requirement to lower the ferromagnetic spin-exchange interaction, which reaches its lowest value if the spin is fully polarized. Combined with the property of $f_z(\mathbf{r}) = 0$, we immediately obtain $n_0 = 2n_1 = 2n_{-1}$ everywhere. Such a density distribution distinguishes the SMA and the FCLSV states from the PCV state where $n_0/n_{1,-1}$ is not a constant, especially around the vortex core.

Typical spatial phase and spin density distributions of a FCLSV are presented in Fig. 3. As a comparison, we also show the constant spatial phase and spin density distributions of an SMA state. The spatial phases of the $|0\rangle$ component of the FCLSV and the SMA are not shown because they are trivially constant. Clearly, the phases of the FCLSV linearly change $\mp 2\pi$ around the origin for the $|1\rangle$ and $|-1\rangle$ components, respectively, illustrating the phase distribution of a spin vortex. This phase changing is distinctive from the SMA, whose phases are constant in the whole space. The spin density distribution in Fig. 3(f) shows more direct evidence, where the local spins are aligned circularly around the center of the spin vortex. Clearly, the spin direction (along the azimuthal angle) is always perpendicular to the density gradient, which has nonzero components only along the radial direction and the z axis. Such a spin configuration guarantees $E'_{dd} = 0$ (as confirmed also in Fig. 4).

For a vortex, the winding number of the spin component must be a nonzero integer. For the spin vortex, either the PCV or the FCLSV, we calculate the winding number of each spin component, which is proportional to the angular momentum [28,41]

$$L_m = \frac{\int d\mathbf{r}\, \psi_m^*(\mathbf{r})\big(-i\frac{\partial}{\partial\varphi}\big)\psi_m(\mathbf{r})}{\int d\mathbf{r}|\psi_m(\mathbf{r})|^2}, \quad m = 1, 0, -1. \tag{16}$$

The L_m is depicted in Fig. 4 where U_0 increases from 0 to 200. The abrupt change of winding number from zero to ± 1 is obvious evidence of a topological phase transition. For the ^{87}Rb dipolar spinor condensate, the winding numbers are -1, 0, and 1 for the three components $|1\rangle$, $|0\rangle$, and $|-1\rangle$, respectively, in the spin vortex phase where the optical-plug barrier height U_0 is large.

The phase transition from the SMA to the spin vortex is also indicated by the density ratios for the $|\pm 1\rangle$ component $R_{1,-1}$, which is defined as $R_{1,-1} = n_{1,-1}(0, 0, 0)/n_p$. Since $f_z = 0$ everywhere, $n_1 = n_{-1}$ and thus $R_1 = R_{-1}$ always holds. In the spin vortex phase, $R_{1,-1} = 0$ indicates that the densities of the $|\pm 1\rangle$ component are zero at the vortex core.

As we discussed in Sec. III, the spin vortex in the dipolar spinor BEC may be ascribed to the competition between the

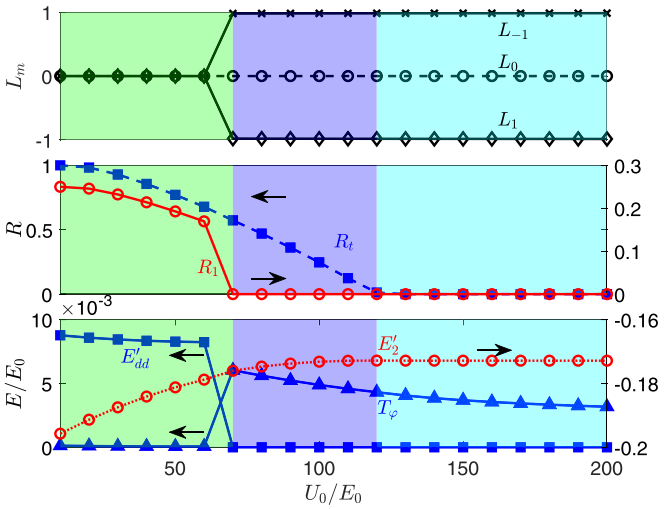

FIG. 4. Phase transitions induced by the plug with the same parameters as in Fig. 2. The phase transition from the SMA (light green) to the PCV (light blue) occurs at $U_0 = 70$, where L_{-1} (solid line with crosses), L_1 (solid line with diamonds), R_1 (solid line with circles), E'_{dd} (solid line with squares), and T_φ (solid line with triangles) undergo an obvious disruption. The structure change from the PCV to the FCLSV (cyan) occurs at $U_0 = 120$, where R_t approaches zero. The L_0 (dashed line with circles) is always zero and E'_2 (dotted line with circles) is continuous and smooth at both phase transitions.

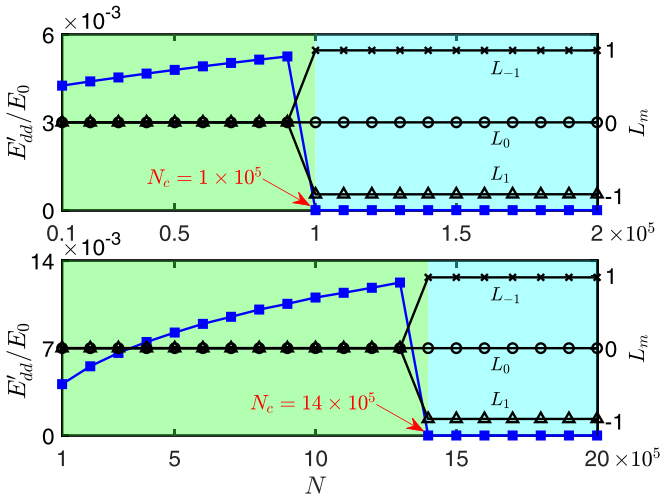

FIG. 5. Same as Fig. 4 except on the atom number N for $U_0 = 90$ with (top) and without (bottom) an optical plug. The critical atom number N_c (red arrow) with the optical plug is an order of magnitude lower than that without the optical plug.

kinetic energy along the azimuthal angle

$$T_\varphi = \sum_{m=-1,0,1} \int d\mathbf{r}\, \psi_m^*(\mathbf{r}) \left(-\frac{\partial^2}{2\rho^2 \partial \varphi^2} \right) \psi_m(\mathbf{r})$$

and the intrinsic dipolar energy E'_{dd}. Indeed, the intrinsic dipolar energy drops suddenly to zero, but the azimuthal kinetic energy soars from zero around the phase transition. More importantly, the sum energy $E'_{dd} + T_\varphi$ also decreases abruptly once the system changes from the SMA phase to the spin vortex, provided other spin energy terms like E'_2 remain continuous and smooth. This confirms that the spin vortex is due to nothing but the MDDI effect.

As the optical-plug potential barrier height U_0 further increases, the dipolar BEC changes from the PCV to the FCLSV indicated by the total density ratio R_t, which is defined as $R_t = n(0,0,0)/n_p$. Such a gradual change in the central total density is manifested by the appearance of the coreless vortex, i.e., $n(0,0,0) = 0$. Obviously, the FCLSV is distinguished from the PCV where a polar core exists $[n_0(0,0,0) \text{is nonzero though} n_{1,-1}(0,0,0) = 0]$.

More atoms in the ^{87}Rb dipolar BEC is good for the formation of a spin vortex structure [28]. We investigate also the phase transition for the atom number N. The numerical results are shown in Fig. 5. The calculation box $R_{x,y,z}$ is adjusted appropriately with N increasing. Clearly, the spin vortex always appear if the number of atoms is larger than a critical value N_c, with or without an optical plug. However, the critical atom number N_c with an optical plug is an order of magnitude smaller than that without the optical plug ($1.4 \times 10^6 \to 1 \times 10^5$). Therefore, the application of an additional optical plug mitigates greatly the experimental effort to realize a spin vortex in the ^{87}Rb dipolar spinor BEC.

VI. CONCLUSION

By increasing the potential barrier height and adjusting appropriately the width of an additionally applied optical plug, a ^{87}Rb dipolar spinor condensate transits from a spin-uniform SMA phase to a spin vortex one, due to the competition between the MDDI and the azimuthal kinetic energy. With the aid of the optical plug, it is possible to generate the PCV and the FCLSV states of the ^{87}Rb dipolar condensate in a controllable way under more relaxed experimental conditions, e.g., an order of magnitude smaller atom number and smaller aspect ratio. Our results provide a practical way to realize the spin vortex state and to explore the topological quantum phase transition and dynamical phase transitions in ^{87}Rb condensates.

Recent experiments in a ferromagnetic spin-1 ^{7}Li BEC demonstrated a very large spin-dependent exchange interaction strength ($|c_2| \sim c_0/2$) [56–58]. For such a strong ferromagnetic interaction, it would be more challenging to generate a spin vortex state. However, as implied by Eq. (10), a FCLSV state is still possible with the assistance of an optical plug. It is wort exploring this novel regime in the future.

ACKNOWLEDGMENTS

This work was supported by the National Natural Science Foundation of China under Grants No. U1930201, No. 12135018, and No. 91836101.

APPENDIX: DERIVATION OF EQ. (10)

In the quasi-one-dimensional ring trap, we assume that the ring of a BEC lies in the two-dimensional plane with a linear density $n = N/2\pi\sigma$, where σ is the ring's radius. For the ^{87}Rb dipolar BEC, the one-dimensional wave function

is expressed as $\psi_m(\varphi) = (1/\sqrt{2\pi})\exp(i\theta_m)$ $(m = 1, 0, -1)$, where the phase $\theta_m = k_m\varphi + \alpha_m$ satisfies [14,59]

$$\theta_1 + \theta_{-1} - 2\theta_0 = 0. \tag{A1}$$

For the spin vortex we consider, $k_m = -m$, and for the SMA phase $k_m = 0$ [27].

We calculate the energy difference ΔE between two local-energy-minimum states, the SMA and the spin vortex state, denoted by the superscripts S and V, respectively. Due to the homogeneous one-dimensional density, the potential energy difference $\Delta V \equiv V^V - V^S = 0$ and the spin-independent (density) interaction energy difference $\Delta E_0 = 0$. The kinetic energy is

$$T = \sum_m \int \sigma\, d\varphi\, \psi_m^*\left(-\frac{1}{2\sigma^2}\frac{\partial^2}{\partial\varphi^2}\right)\psi_m = \frac{1}{2\sigma^2}\sum_m \zeta_m k_m^2, \tag{A2}$$

where N_m is the atom number of the m component and $\zeta_m = N_m/N$. Clearly, $T^S = 0$ and thus the kinetic energy difference $\triangle T = T^V - T^S = T^V = (\zeta_1 + \zeta_{-1})/2\sigma^2$.

To calculate the MDDI energy difference, we cut off the dipolar interaction at the average distance of two neighboring atoms $r_c = 2\pi\sigma/N$ [48], which yields the cutoff of the azimuthal angle $\varphi_c = 2\pi/N$ on the ring. The MDDI energy difference is

$$\begin{aligned}\triangle E_{dd} &= E_{dd}^V - E_{dd}^S \\ &= -\frac{c_{dd}N}{16\pi^2\sigma^3}\int_{\varphi_i}^{\varphi_f} d\varphi_- \\ &\quad\times \int_0^{2\pi} d\varphi_+ \frac{3 - 2\sin^2(\varphi_-) + 3\cos(2\varphi_+)}{|\sin(\varphi_-)|^3} \\ &= -\frac{c_{dd}N}{8\pi\sigma^3}\int_{\varphi_i}^{\varphi_f} d\varphi_- \frac{3 - 2\sin^2(\varphi_-)}{|\sin(\varphi_-)|^3} \\ &= -\frac{c_{dd}N}{8\pi\sigma^3} I_{dd},\end{aligned} \tag{A3}$$

where $\varphi_i = \varphi_c$, $\varphi_f = 2\pi - \varphi_c$, and $\varphi_\pm = (\varphi \pm \varphi')/2$, with φ and φ' representing the azimuthal angle of two atoms located at (σ, φ) and (σ, φ'), respectively. Obviously, I_{dd} is only a positive number determined by the atom number and the truncation φ_c. As a result, the total energy difference becomes

$$\triangle E = \triangle T + \triangle E_{dd} = \frac{\zeta_1 + \zeta_{-1}}{2\sigma^2} - \frac{c_{dd}N}{8\pi\sigma^3} I_{dd}. \tag{A4}$$

[1] H. Nishimori and G. Ortiz, *Elements of Phase Transitions and Critical Phenomena* (Oxford University Press, Oxford, 2011).
[2] H. K. Onnes, Commun. Phys. Lab. Univ. Leiden **120b** (1911).
[3] V. F. Gantmakher and V. T. Dolgopolov, Phys. Usp. **53**, 1 (2010).
[4] N. Majlis, *The Quantum Theory of Magnetism* (World Scientific, Hackensack, 2001).
[5] K. Von Klitzing, G. Dorda, and M. Pepper, Phys. Rev. Lett. **45**, 494 (1980).
[6] S. Sachdev, *Quantum Phase Transitions* (Cambridge University Press, Cambrige, 1999).
[7] G. Chen, J.-Q. Liang, and Z. Chen, Europhys. Lett. **79**, 10001 (2007).
[8] X.-Y. Luo, Y.-Q. Zou, L.-N. Wu, Q. Liu, M.-F. Han, M. K. Tey, and L. You, Science **355**, 620 (2017).
[9] P. Xu, S. Yi, and W. Zhang, Phys. Rev. Lett. **123**, 073001 (2019).
[10] D. M. Stamper-Kurn, M. R. Andrews, A. P. Chikkatur, S. Inouye, H.-J. Miesner, J. Stenger, and W. Ketterle, Phys. Rev. Lett. **80**, 2027 (1998).
[11] T. Ohmi and K. Machida, J. Phys. Soc. Jpn. **67**, 1822 (1998).
[12] T.-L. Ho, Phys. Rev. Lett. **81**, 742 (1998).
[13] C. K. Law, H. Pu, and N. P. Bigelow, Phys. Rev. Lett. **81**, 5257 (1998).
[14] S. Yi, Ö. E. Müstecaplıoğlu, C. P. Sun, and L. You, Phys. Rev. A **66**, 011601(R) (2002).
[15] D. M. Stamper-Kurn and M. Ueda, Rev. Mod. Phys. **85**, 1191 (2013).
[16] Y. Kawaguchi and M. Ueda, Phys. Rep. **520**, 253 (2012).
[17] W. Alt, D. Schrader, S. Kuhr, M. Müller, V. Gomer, and D. Meschede, Phys. Rev. A **67**, 033403 (2003).
[18] M. D. Barrett, J. A. Sauer, and M. S. Chapman, Phys. Rev. Lett. **87**, 010404 (2001).
[19] S. Yi, L. You, and H. Pu, Phys. Rev. Lett. **93**, 040403 (2004).
[20] S. Yi and L. You, Phys. Rev. A **66**, 013607 (2002).
[21] K. Góral, L. Santos, and M. Lewenstein, Phys. Rev. Lett. **88**, 170406 (2002).
[22] K. Góral, K. Rzążewski, and T. Pfau, Phys. Rev. A **61**, 051601(R) (2000).
[23] T. Lahaye, C. Menotti, L. Santos, M. Lewenstein, and T. Pfau, Rep. Prog. Phys. **72**, 126401 (2009).
[24] J. Stuhler, A. Griesmaier, T. Koch, M. Fattori, T. Pfau, S. Giovanazzi, P. Pedri, and L. Santos, Phys. Rev. Lett. **95**, 150406 (2005).
[25] M. Vengalattore, S. R. Leslie, J. Guzman, and D. M. Stamper-Kurn, Phys. Rev. Lett. **100**, 170403 (2008).
[26] M. Lu, N. Q. Burdick, S. H. Youn, and B. L. Lev, Phys. Rev. Lett. **107**, 190401 (2011).
[27] S. Yi and H. Pu, Phys. Rev. Lett. **97**, 020401 (2006).
[28] Y. Kawaguchi, H. Saito, and M. Ueda, Phys. Rev. Lett. **97**, 130404 (2006).
[29] J. A. M. Huhtamäki, M. Takahashi, T. P. Simula, T. Mizushima, and K. Machida, Phys. Rev. A **81**, 063623 (2010).
[30] L. Sadler, J. Higbie, S. Leslie, M. Vengalattore, and D. Stamper-Kurn, Nature (London) **443**, 312 (2006).
[31] H. Saito, Y. Kawaguchi, and M. Ueda, Phys. Rev. A **75**, 013621 (2007).
[32] K. B. Davis, M. O. Mewes, M. R. Andrews, N. J. van Druten, D. S. Durfee, D. M. Kurn, and W. Ketterle, Phys. Rev. Lett. **75**, 3969 (1995).
[33] T. W. Neely, E. C. Samson, A. S. Bradley, M. J. Davis, and B. P. Anderson, Phys. Rev. Lett. **104**, 160401 (2010).
[34] H. Fu, M. Li, B. Gao, and Y. Wang, Phys. Lett. A **308**, 471 (2003).
[35] Y. Kawaguchi, H. Saito, K. Kudo, and M. Ueda, Phys. Rev. A **82**, 043627 (2010).

[36] S. Yi and H. Pu, Phys. Rev. A **73**, 023602 (2006).
[37] T. Li, S. Yi, and Y. Zhang, Phys. Rev. A **93**, 053602 (2016).
[38] S.-X. Deng, T. Shi, and S. Yi, Phys. Rev. A **102**, 013305 (2020).
[39] W. Bao and Y. Cai, Kinet. Relat. Mod. **6**, 1 (2013).
[40] K. Góral and L. Santos, Phys. Rev. A **66**, 023613 (2002).
[41] H. Saito, Y. Kawaguchi, and M. Ueda, Phys. Rev. Lett. **96**, 065302 (2006).
[42] C.-M. Schmied, T. Gasenzer, and P. B. Blakie, Phys. Rev. A **100**, 033603 (2019).
[43] L. A. Williamson and P. B. Blakie, Phys. Rev. Research **3**, 013154 (2021).
[44] L. A. Williamson and P. B. Blakie, Phys. Rev. A **94**, 063615 (2016).
[45] J. A. Kjäll, A. M. Essin, and J. E. Moore, Phys. Rev. B **80**, 224502 (2009).
[46] M. Ueda, *Fundamentals and New Frontiers of Bose-Einstein Condensation* (World Scientific, Singapore, 2010).
[47] D. S. Naik and C. Raman, Phys. Rev. A **71**, 033617 (2005).
[48] S. Yi and L. You, Phys. Rev. A **63**, 053607 (2001).
[49] V. Yukalov and E. Yukalova, Laser Phys. **26**, 045501 (2016).
[50] V. Yukalov, Laser Phys. **28**, 053001 (2018).
[51] A. S. Arnold, C. S. Garvie, and E. Riis, Phys. Rev. A **73**, 041606(R) (2006).
[52] S. Beattie, S. Moulder, R. J. Fletcher, and Z. Hadzibabic, Phys. Rev. Lett. **110**, 025301 (2013).
[53] T. Shi, E. Demler, and J. I. Cirac, Ann. Phys. (NY) **390**, 245 (2018).
[54] S. Ronen, D. C. E. Bortolotti, and J. L. Bohn, Phys. Rev. A **74**, 013623 (2006).
[55] W. Bao, D. Jaksch, and P. A. Markowich, J. Comput. Phys. **187**, 318 (2003).
[56] S. J. Huh, K. Kim, K. Kwon, and J. Y. Choi, Phys. Rev. Research **2**, 033471 (2020).
[57] K. Kwon, K. Mukherjee, S. J. Huh, K. Kim, S. I. Mistakidis, D. K. Maity, P. G. Kevrekidis, S. Majumder, P. Schmelcher, and J.-y. Choi, Phys. Rev. Lett. **127**, 113001 (2021).
[58] K. Kim, J. Hur, S. J. Huh, S. Choi, and J. Y. Choi, Phys. Rev. Lett. **127**, 043401 (2021).
[59] T. Isoshima, K. Machida, and T. Ohmi, J. Phys. Soc. Jpn. **70**, 1604 (2001).

Correction: Table I was erroneously modified during production and has been fixed.